Intralayer and interlayer energy transfer from excitonic states into the Mn $3d^5$ shell in diluted magnetic semiconductor structures

H. Falk, J. Hübner, P. J. Klar,* and W. Heimbrodt

Department of Physics and Material Sciences Center, Philipps-University, Renthof 5, D-35032 Marburg, Germany
(Received 25 March 2003; published 17 October 2003)

We show that the Dexter-Förster-like radiationless resonance energy-transfer process from excitonic states into the Mn $3d^5$ shell in wide-gap (II,Mn)VI semiconductors is strongly enhanced if the total spin of the overall process is conserved. This requirement cannot be fulfilled in processes involving a bright exciton, i.e., other excitonic complexes or processes need to be involved. Of these we discuss dark excitons, donor-bound excitons D^0X, negatively charged excitons X^-, and an Auger-like process. A careful analysis of the magnetic field and time dependence of the excitonic and Mn luminescence in the (Zn,Cd,Mn)Se samples under study gives evidence that the D^0X complex plays a dominant role in the intralayer energy transfer. In asymmetric double quantum well (ADQW) structures consisting of a (Zn,Cd)Se well and a (Zn,Cd,Mn)Se well embedded in ZnSe barriers, there is a competition between the intralayer and interlayer energy-transfer processes from excitonic states into the Mn system. These interlayer processes take place between the Mn ions situated in the (Zn,Cd,Mn)Se well and spatially indirect excitons [where the hole is confined in the (Zn,Cd,Mn)Se and the electron confined in the (Zn,Cd)Se] as well as spatially direct excitons of the (Zn,Cd)Se well. The continuous magnetic-field tuning demonstrates convincingly the subtle interplay of excitonic band structure of the ADQW and spin effects in the energy-transfer processes. A spin-dependent energy transfer should be a general feature of rare-earth or transition-metal doped semiconductors such as II-VI or III-V semiconductors or even Er-doped Si or SiO_2.

I. INTRODUCTION

Diluted magnetic semiconductors (DMS's; more often referred to as semimagnetic semiconductors) are useful tools for studying basic physical problems in semiconductor structures. The strong exchange interaction between the localized magnetic moments of the Mn^{2+} ions and the extended band states ($s,p\text{-}d$ exchange interaction) yields the "giant"-Zeeman splitting. Therefore a continuous tuning by an external magnetic field of important parameters such as the band-gap energy or barrier heights in quantum well structures becomes feasible over an energy range of the order of 100 meV. This enables one to study in detail the dependence on such a tuning parameter of, for example, interwell coupling or tunneling processes of carriers and excitons in one and the same sample.[1–5]

Another point of intensive discussion is the energy-transfer mechanism from band or exciton states into the internal transitions of transition metals (TM's) or rare earths (RE's). This mechanism of the energy transfer is an essential question not only for doped II-VI semiconductors but also for other systems like Er-doped Si or SiO_2 as well as III-V semiconductors doped by TM or RE ions where dipole forbidden internal transitions can be effectively excited via band states. Although it has been known for decades that this energy transfer in wide band-gap DMS's from the excitonic states into the internal Mn^{2+} ($3d^5$) shell is extremely effective the underlying mechanism is not at all understood.[6–10] The Mn^{2+} ions are incorporated on cation sites of the II-VI hosts. The tetrahedral crystal field of the cation site shifts and splits the $3d$ states in energy compared to the free Mn^{2+} ion. The ^6S ground state of the free Mn^{2+} ion (which according

to Hund's rule has all five electron spins aligned parallel giving rise to a total spin $S = \frac{5}{2}$) is shifted down in energy by the crystal field and is referred to as $^6A_1$. The first excited quartet state ^4G of the free ion is split into four states which with increasing energy are labeled according to the irreducible representation of T_d symmetry by $^4T_1$, $^4T_2$, $^4A_1$, and ^4E (all having a total spin of $S = \frac{3}{2}$). In wide gap (Cd,Mn) and (Zn,Mn) chalcogenide alloys the effective energy transfer is manifested by a broad orange luminescence band due to the transition from $^4T_1$ first excited state to the $^6A_1$ ground state of the Mn $3d$ shell which is observed in addition to, or even instead of, the excitonic emission.[11–13] This transition occurs although the internal optical transitions within the d shell are in principle forbidden by parity and spin selection rules. Various mechanisms for a weakening of these selection rules have been discussed, which eventually lead to finite transition probabilities and finite lifetimes. For smallest Mn concentrations and dominantly isolated Mn-ion centers the decay time of the $^4T_1 \rightarrow {}^6A_1$ transition was found to be about 1.8 ms,[14] and reduces into the μs range with increasing Mn concentration, mainly caused by the so-called "concentration quenching."[15,16] The most likely mechanisms for the relaxation of the selection rules are the spin-orbit coupling, the $p\text{-}d$ hybridization of the Mn $3d^5$ states with the p states of the surrounding anions, and the lack of inversion symmetry.[12,17]

In Sec. III of the paper we will deal with the energy transfer between excitons and Mn ions when both are situated in the same layer, i.e., intralayer energy transfer. We will show by studying the magnetic field and time dependence of the luminescence that, although the spin selection rule is somewhat relaxed, it is still of special relevance for the radiation-

TABLE I. Sample parameters.

Sample A	MQW	5
	corresponding QD ($\varnothing$ 140 nm)	$\times$\{22 nm ZnSe/24 nm $Zn_{0.75}Cd_{0.16}Mn_{0.09}Se$\}/900 nm ZnSe/ (100) GaAs substrate
Sample B	ADQW	20 nm ZnSe/6 nm $Zn_{0.67}Cd_{0.18}Mn_{0.15}Se$/6 nm ZnSe/ 6 nm $Zn_{0.82}Cd_{0.18}Se$/1000 nm ZnSe/(100) GaAs substrate
Sample C	ADQW	20 nm ZnSe/6 nm $Zn_{0.76}Cd_{0.15}Mn_{0.09}Se$/6 nm ZnSe/ 6 nm $Zn_{0.85}Cd_{0.15}Se$/1000 nm ZnSe/(100) GaAs substrate

less energy transfer into the $3d^5$ shell of the Mn^{2+} ions. Usually the energy resonance between the initial and the final state is discussed as the only important condition for the energy transfer in a Dexter-Förster-like mechanism. Our results clearly show that besides the resonance condition the spin selection rule also plays an important role. It is noteworthy that the actual underlying mechanism of the energy transfer is not relevant for our discussion. The most likely mechanisms are dipole-dipole transfer and the exchange interaction. Of importance is, however, that the initial as well as the final state can be observed as dipole transitions in wide band-gap semiconductors. This is the difference to phenomena discussed in narrow gap DMS where an effective spin heating of the Mn subsystem caused by a spin-flip scattering process via electron-Mn exchange interaction was observed.[18]

In Sec. IV of the paper we will extend our studies to energy-transfer processes between excitons and magnetic ions in asymmetric double quantum well structures (ADQW's) consisting of a nonmagnetic quantum well (NMW) and a diluted magnetic quantum well (DMW). By making use of continuous tuning of the band alignment of such ADQW's by an external magnetic field, we will demonstrate that there is a competition between the intralayer processes discussed in Sec. III and interlayer energy-transfer processes. The interlayer processes take place between the Mn ions situated in the DMW and indirect excitons (where the hole is confined in the DMW and the electron confined in the NMW) as well as direct excitons of the NMW. The continuous magnetic-field tuning demonstrates convincingly the subtle interplay of excitonic band structure of the ADQW and spin effects in the energy-transfer processes. Section V will conclude the paper.

II. SAMPLE PREPARATION AND EXPERIMENTAL DETAILS

The experimental data in Sec. III concerning the intralayer energy transfer were obtained from sample A, a $Zn_{0.75}Cd_{0.16}Mn_{0.09}Se$/ZnSe multiple quantum well (MQW) structure grown by molecular beam epitaxy (MBE). The structure consisted of five 24-nm-wide $Zn_{0.75}Cd_{0.16}Mn_{0.09}Se$ layers separated by 22-nm ZnSe barriers. The sample was grown pseudomorphicly on a (100) GaAs substrate. Part of this parent sample was used to fabricate quantum disc (QD) structures. The nanofabrication process is described in detail elsewhere.[19,20] In brief, the pattern was defined by electron-

beam lithography and was transferred by argon-ion beam etching followed by wet-chemical etching. The disc diameters were determined to be about 140 nm by atomic force microscopy and scanning electron microscopy. Two MBE-grown asymmetric double quantum well structures (ADQW's) were used for studying the interlayer energy transfer in Sec. IV. Again both samples were grown on (100) GaAs substrates. Sample B consisted of a 6-nm $Zn_{0.82}Cd_{0.18}Se$ nonmagnetic quantum well (NMW) separated by a 6-nm ZnSe barrier from a 6-nm $Zn_{0.67}Cd_{0.18}Mn_{0.15}Se$ diluted magnetic quantum well (DMW). Sample C is of the same structure as sample B, but has slightly different Mn and Cd concentrations in the QW's: $Zn_{0.85}Cd_{0.15}Se$ and $Zn_{0.76}Cd_{0.15}Mn_{0.09}Se$ for the NMW and the DMW, respectively. In both samples the DMW was grown after the NMW. The sample parameters are summarized in Table I. The continuous-wave photoluminescence (PL) and PL excitation (PLE) measurements were carried out at 2 K using a superconducting magnet system with a maximum field of up to 7.5 T. As excitation sources served a HeCd laser (442 nm) and a tunable dye-laser (Coumarin 47). The PL spectra were detected using a single grating spectrometer equipped with a liquid-nitrogen-cooled charge-coupled device detector. The PLE spectra were recorded detecting either on the QW excitonic emission or on the orange Mn-luminescence band. Picosecond (ps) PL experiments were carried out at 6 K using a different superconducting magnetic system with fields up to 14 T. A mode-locked Ti:sapphire laser was used for excitation and a streak-camera system for detection. Two different magnetic-field geometries were employed: a Faraday-type geometry ($B\|k$ and $z\|B$; where k is the propagation vector of the detected light and z is the growth direction, which is perpendicular to the biaxially strained crystallographic plane) and a Voigt-type geometry ($B\perp k\|z$ and $z\perp B\|x$). This Voigt-type geometry should not be confused with that usually used in bulk samples ($z\|B$ and $k\|x$). Polarization optics were used to distinguish between the two circular polarizations and the two linear polarizations in Faraday and Voigt geometry, respectively.

III. INTRALAYER ENERGY TRANSFER

A. Experimental findings

Figure 1(a) depicts PL spectra of sample A and the corresponding QD sample. Two main signals are observable in the two spectra. A sharp band at about 2.6 eV corresponding to the excitonic emission of the $Zn_{0.75}Cd_{0.16}Mn_{0.09}Se$ QW or

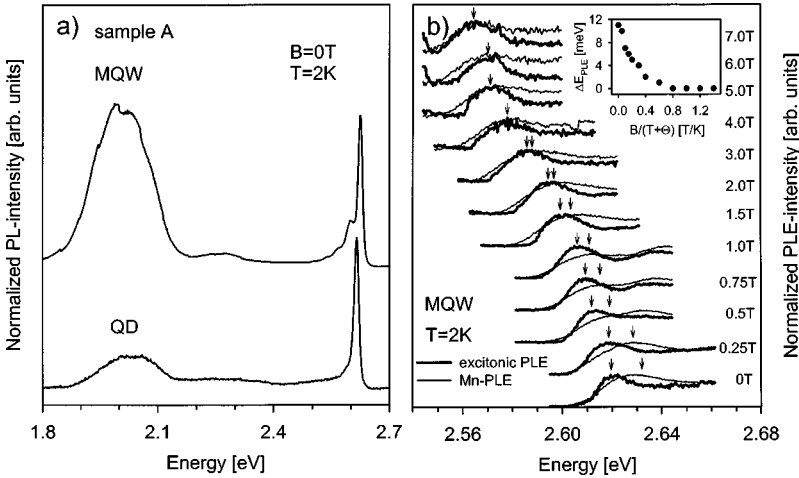FIG. 1. (a) Photoluminescence (PL) spectra of a $Zn_{0.75}Cd_{0.16}Mn_{0.09}Se/ZnSe$ multiple quantum well (MQW) and of the corresponding quantum disc (QD) sample. $B = 0$ T, $T = 2$ K. (b) σ^+ PL excitation (PLE) spectra recorded at various magnetic fields up to 7 T. Thick lines and thin lines correspond to PLE spectra detected on the excitonic PL (at about 2.6 eV) and the Mn PL (at about 2 eV). $T = 2$ K. Inset: Energy shift between the PLE peaks recorded on excitonic and Mn PL as a function of effective magnetic field.

QD layers. Some general remarks about the excitonic PL emission in these samples are necessary for the following discussion. These quaternary alloys have an intrinsically large PL linewidth of about 10 meV at zero-magnetic field. The broad PL band referred to as the excitonic emission actually consists of two unresolved emission bands, separated by a few meV, that of the free exciton (*FX*) and that of the donor bound exciton D^0X. This has been confirmed by careful analysis of the total linewidth as a function of magnetic field and QD size.[26,30] The intensities of the *FX* and the D^0X are affected by the nanofabrication as well as by applying an external magnetic field. As shown previously in Ref. 20 for $ZnSe/Zn_{1-x}Mn_xSe$ MQW and QD samples, the intensity ratio of D^0X to *FX* emission in zero-magnetic field decreases drastically with decreasing QD diameter because, statistically, the number of QD pillars without donor ions increases. On applying an external magnetic field, the intensity behavior of the D^0X and the *FX* bands is very different because of the destabilization of the D^0X.[27] These effects are discussed in more detail below. The second PL band centered at about 2 eV corresponds to the orange internal Mn luminescence from $^4T_1$ first excited state to the $^6A_1$ ground state of the Mn $3d^5$ shell. The relative intensity of the Mn band in the QD samples is much weaker than in the corresponding parent structure. Nevertheless, in both spectra the broad Mn band almost dominates although the internal transition is dipole forbidden by spin and parity selection rules. This indicates that the intralayer energy transfer from the excitonic states to the Mn subsystem is very efficient and represents a competing effect to the radiative recombination process of the excitons in the layer. This is further confirmed by Fig. 1(b) which shows PLE spectra recorded in Faraday geometry at magnetic fields up to 7 T of the spectral range of the σ^+ component of the heavy-hole exciton. The thick lines and the thin lines correspond to PLE spectra detected either on the excitonic emission or on the orange Mn-emission band. The corresponding PL spectra are shown in Fig. 2. Both types of PLE spectra in Fig. 1(b) show clear features of the heavy-hole exciton. The existence of such features in the PLE spectra recorded on the Mn band is clear evidence that an energy transfer from the excitonic states into the Mn $3d^5$ shells takes place at all magnetic fields up to 7 T. With increasing

magnetic field the σ^+ component of the heavy-hole exciton shifts strongly to lower energies due to the *s,p-d* exchange interaction induced giant Zeeman splitting. The shift is proportional to the Brillouin function $B_{5/2}$ of the average component $\langle S_\parallel \rangle$ of the Mn spin aligned along the magnetic-field direction given by

$$\langle S_\parallel \rangle = aSB_{5/2}(\zeta),$$

$$B_{5/2}(\zeta) = \frac{6}{5}\coth\left(\frac{6\zeta}{5}\right) - \frac{1}{5}\coth\left(\frac{\zeta}{5}\right), \qquad (1)$$
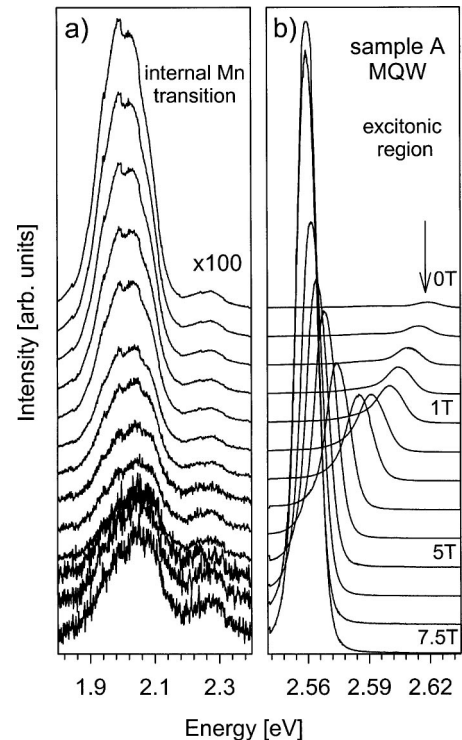
where

FIG. 2. (a) Magneto-PL spectra of the $Zn_{0.75}Cd_{0.16}Mn_{0.09}Se/ZnSe$ MQW. (a) Mn PL; (b) excitonic PL. $T = 2$ K. Excitation energy was 2.81 eV.
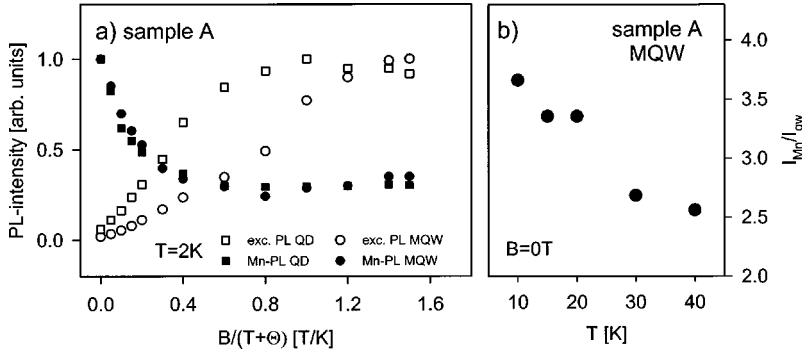
FIG. 3. (a) Dependence of the relative intensities of excitonic and Mn PL on effective magnetic field for the $Zn_{0.75}Cd_{0.16}Mn_{0.09}Se/ZnSe$ MQW and for the corresponding QD's. (b) Temperature dependence of the intensity ratio of Mn PL and excitonic PL at $B = 0$ T.

$$\zeta = \frac{g'\mu_B S B}{k(T+\Theta)}. \tag{2}$$

The empirical parameters a and Θ account for the antiferromagnetic d-d coupling between the spins of the Mn ions. A fit of the corresponding energy dependence on the magnetic field (not shown here) leads to $T+\Theta = 5$ K. For better comparability of results recorded at different temperatures T, it is useful to introduce an effective magnetic-field parameter B_{eff} defined as

$$B_{eff} = \frac{B}{T+\Theta}. \tag{3}$$

The excitation bands in Fig. 1(b) recorded on both luminescence bands in Fig. 2 show differences in their magnetic-field dependence. Already at zero field the peak of the excitation band recorded on the Mn luminescence is about 10 meV higher in energy than the corresponding peak detected on the excitonic band. With increasing magnetic field the energy difference between the two peak positions decreases rapidly and starts to level off at $B_{eff} = 0.6$ T/K as shown in the inset of Fig. 1(b).

Figure 3(a) shows the integrated intensities of the Mn band and the excitonic PL for sample A and the corresponding QD sample as a function of B_{eff} derived from PL spectra recorded in Faraday geometry (see Fig. 2 for the MQW). In both samples, the Mn PL decreases strongly up to about $B_{eff} = 0.6$ T/K and remains constant at higher fields for both samples. The excitonic PL of the MQW basically increases over the whole range, whereas the QD PL increases and then saturates at about $B_{eff} = 0.8$ T/K. A similar suppression of the energy transfer from the excitonic states into the Mn subsystem by an external magnetic field has been observed for self-assembled CdSe quantum dots in a (Zn,Mn)Se matrix.[21] Figure 3(b) shows the temperature dependence of the intensity ratio of the Mn PL and the excitonic PL for zero field of sample A. It can be seen that the ratio decreases strongly with increasing temperature.

As the Mn recombination and the excitonic recombination are the final processes of competing radiative relaxation paths after barrier excitation, it is obvious that the change of the relative intensities of the corresponding PL bands in the external magnetic field should be reflected in the dynamics of the excitonic emission, i.e., the decay time of the excitonic states will be affected by the magnetic-field-induced changes of the energy transfer into the Mn $3d^5$ states. Picosecond PL

spectra were recorded in Faraday as well as in Voigt geometry at a temperature of 6 K. By spectral integration of the PL band the excitonic decay curves were derived. These are shown in Fig. 4 for sample A. It is clearly seen that the decay is strongly reduced with increasing field. The decay time τ were obtained by fitting the experimental data using the following equation:

$$I(t) = I_0 \cdot \left[-\exp\left(-\frac{t}{\tau}\right) + \exp\left(-\frac{t}{T_{eff}}\right) \right], \tag{4}$$

where the rise time T_{eff} is an effective relaxation time of the carriers from the barrier into the quantum well which is assumed to be independent of the magnetic field. The fit yields T_{eff} of about 5 ps. The decay times τ for sample A are plotted in the Fig. 5(a) as a function of B_{eff}. For both configurations the decay time increases with increasing B_{eff} but exhibits a tendency to saturate at about 0.6 T/K in the Faraday configu-
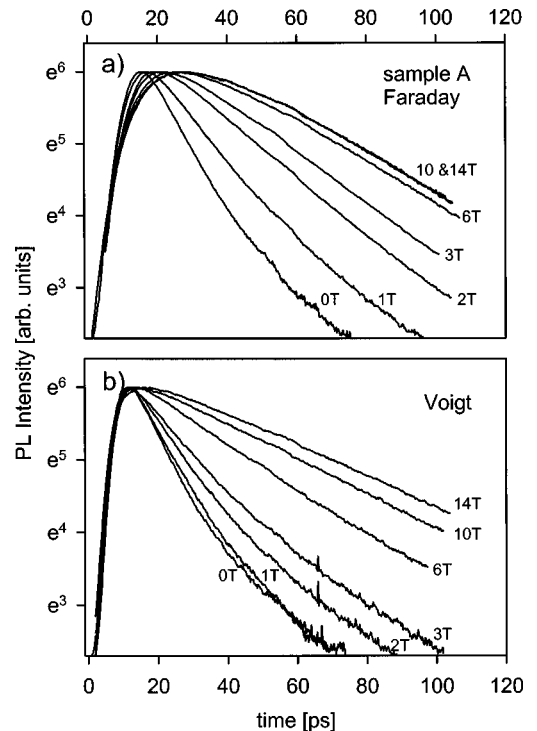

FIG. 4. Experimental decay curves of the spectrally integrated intensity of sample A in (a) Faraday and (b) Voigt configuration for various magnetic fields. $T = 6$ K.
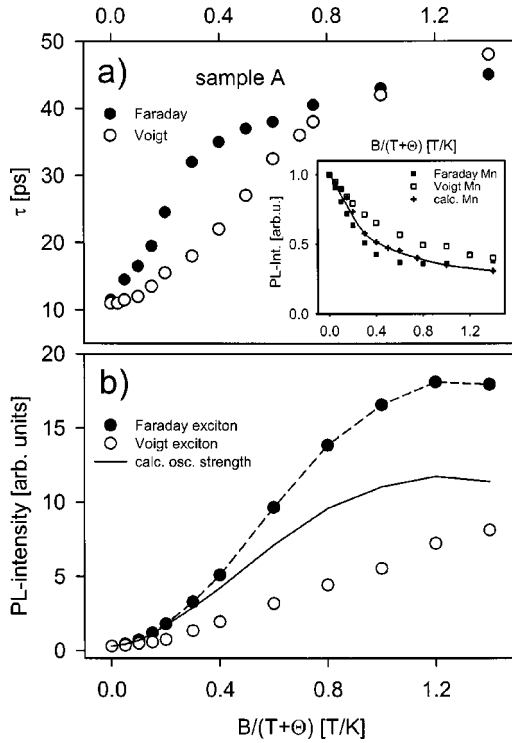
FIG. 5. (a) Decay times of the excitonic PL as a function of effective magnetic field derived by fitting the time dependence of the excitonic PL (Fig. 4) in Faraday (●) and Voigt (○) geometry. Inset: Mn PL intensity as a function of the effective magnetic field in Faraday and Voigt geometry. The crosses denote calculated values for the relative Mn intensity of the MQW derived from the excitonic decay times on the basis of a rate-equation model. The solid line is a guide to the eye. (b) Comparison of the excitonic PL intensity in Faraday (●) and Voigt (○) geometry as a function of the effective magnetic field. The full line is the calculated transition probability for the lowest transition in Voigt configuration taking the dashed to be the respective transition probability in Faraday configuration.

ration. In the intermediate field range the τ values in Voigt configuration are considerably smaller. The decay times increase for both configurations from 11 ps at zero field to about 45 ps at highest field strengths. On the basis of a simple kinetic rate equation model it is possible to correlate the measured excitonic decay times τ and the magnetic-field-induced variation of the Mn-PL intensity. Assuming a constant excitation A of the system by photons the occupation numbers of the excitonic state N_{exc} and the Mn $3d^5$ shell N_{Mn} will be determined by the following two coupled equations:

$$\frac{dN_{exc}}{dt} = A - \frac{N_{exc}}{\tau_r} - \frac{N_{exc}}{\tau_n} - \frac{N_{exc}}{\tau_{transfer}},$$

$$\frac{dN_{Mn}}{dt} = \frac{N_{exc}}{\tau_{transfer}} - \frac{N_{Mn}}{\tau_{Mn}}, \tag{5}$$

where τ_r is the radiative and τ_n is the nonradiative decay time of the excitons. The times $\tau_{transfer}$ and τ_{Mn} denote the transfer time from the excitonic states into the Mn subsystem

and the radiative decay time of the Mn PL. Furthermore, we have assumed that the self-absorption of the Mn subsystem is negligible which is a reasonable assumption for excitation above the band gap of the semiconductor as the band absorption is at least two orders of magnitude bigger than the absorption of the Mn subsystem for Mn concentrations below 10%. In the stationary state ($dN_{exc}/dt = 0, dN_{Mn}/dt = 0$) one obtains

$$I_{Mn} \propto \frac{N_{Mn}}{\tau_{Mn}} = \frac{N_{exc}}{\tau_{transfer}} = \frac{A/\tau_{transfer}}{(1/\tau_{transfer} + 1/\tau_{exc})}, \tag{6}$$

where $\tau_{exc} = (1/\tau_r + 1/\tau_n)^{-1}$. As discussed below, it is reasonable to assume to a first approximation a field independent τ_{exc} in Faraday geometry. This allows one to derive the transfer time $\tau_{transfer}(B)$ as a function of the external field from the experimentally determined decay times $\tau(B)$ via

$$\tau_{transfer}(B) = [1/\tau(B) - 1/\tau_{exc}]^{-1}. \tag{7}$$

In the inset of Fig. 5(a) a fit of I_{Mn} (crosses) is depicted calculated using $\tau_{exc} = 60$ ps in Eq. (6). The calculated field dependence agrees well the experimentally measured Mn PL intensity in Faraday (full squares) configuration. The respective transfer times changes from 14 ps at zero field to 180 ps at 14 T. It is obvious, however, that the experimentally determined Mn-PL intensity is higher in Voigt geometry (open squares) compared to the Mn PL in Faraday geometry. The energy transfer from the excitonic states seems to be more effective in Voigt configuration, which is also reflected by the reduced decay times in this configuration.

The details of the transfer mechanisms will be discussed in Sec. III B. In what follows we want to discuss the physical reasons leading eventually to the more effective energy transfer in Voigt geometry. It is well known that there is a strong magneto-optical anisotropy of the energies of the excitonic states in biaxially strained (II, Mn)VI samples.[22–26] This is solely a valence-band effect as the Γ_6 conduction band is isotropic. The degeneracy of the light- and heavy-hole bands at $k = 0$ is lifted due to the strain in the samples. Thus a quantization direction for light and heavy hole is defined. The quantization directions due to strain and magnetic field coincide in the Faraday geometry. Thus there is no mixing of light and heavy holes with increasing magnetic field. This is no longer the case in the Voigt-type geometry employed here as can be seen from the Hamiltonians of the Γ_8 valence-band states in the $|j, j_z\rangle$ representation in Faraday and Voigt geometry:

$$\mathbf{H}_{Faraday}^{\Gamma_8} = \begin{pmatrix} E_{hh} + 3\Omega & 0 & 0 & 0 \\ 0 & E_{lh} + \Omega & 0 & 0 \\ 0 & 0 & E_{lh} - \Omega & 0 \\ 0 & 0 & 0 & E_{hh} - 3\Omega \end{pmatrix},$$

$$\mathbf{H}_{Voigt}^{\Gamma_8} = \begin{pmatrix} E_{hh} & \sqrt{3}\Omega & 0 & 0 \\ \sqrt{3}\Omega & E_{lh} & 2\Omega & 0 \\ 0 & 2\Omega & E_{lh} & \sqrt{3}\Omega \\ 0 & 0 & \sqrt{3}\Omega & E_{hh} \end{pmatrix}, \tag{8}$$

where the Pidgeon-Brown-type eigenfunctions $\{|3/2, -3/2\rangle_z, |3/2, -1/2\rangle_z, |3/2, +1/2\rangle_z, |3/2, +3/2\rangle_z\}$ are used and $\Omega = |\frac{1}{6} N_0 \beta x \langle S_{\parallel} \rangle|$ where $N_0 \beta$ is the p-d exchange integral and x is the Mn concentration.

In Voigt geometry there is a competition between the perturbations due to strain and magnetic field. Strain alone would yield a quantization in the z direction whereas the sole presence of the magnetic field would lead to a quantization perpendicular to z, e.g., in the x direction. The competing effects result in a mixing of light- and heavy-hole states with increasing external magnetic field causing the magneto-optical anisotropy of the excitons. As a consequence, in our samples, the eigenvalue of the highest valence-band state in the field in Voigt geometry is not that of the Faraday geometry $E_{hh} + 3\Omega$ but $E_1 = \frac{1}{2}(E_{hh} + E_{lh} + 2\Omega) + \sqrt{\frac{1}{4}(E_{hh} - E_{lh} - 2\Omega)^2 + 3\Omega^2}$.[26] The point is that this magnetic-field-induced mixing of light- and heavy-hole states also affects the oscillator strength of the lowest excitonic transitions in Voigt compared to that in Faraday geometry. The excitonic PL intensities are depicted in Fig. 5(b). The intensities changes significantly in comparable measurements carried out in Voigt and Faraday geometry. The magnetic-field-induced relative intensity changes of the excitonic PL in the two geometries can be compared to the calculated relative change of the oscillator strength in the field. We assume that the dashed line (i.e., the experimentally observed intensity change in Faraday geometry) gives the square of the dipole matrix element for the σ^+ transition between the highest valence-band state $|3/2, -3/2\rangle_z$ and the lowest electron state $|1/2, -1/2\rangle_z$ as

$$|\langle \tfrac{1}{2}, -\tfrac{1}{2}|\sigma^+|\tfrac{3}{2}, -\tfrac{3}{2}\rangle_z|^2 = M, \qquad (9)$$

where the dipole operator is $\sigma^+ = (1/\sqrt{2})e(\hat{x} + i\hat{y})$ with e being the charge of the electron, $\hat{x}$ and $\hat{y}$ being the unit vectors along the spatial directions x and y. One can calculate the corresponding square of the dipole matrix element for the lowest excitonic transition in the Voigt-type geometry as the sum of its π and σ contributions. The lowest eigenstate in the conduction band is given by $|1/2, -1/2\rangle_x = (1/\sqrt{2})\{|\tfrac{1}{2}, +\tfrac{1}{2}\rangle_z - |\tfrac{1}{2}, -\tfrac{1}{2}\rangle_z\}$ and the highest valence-band eigenstate is that for the eigenenergy E_1:

$$|VB\rangle_x = N_{hh}\{|\tfrac{3}{2}, +\tfrac{3}{2}\rangle_z + |\tfrac{3}{2}, -\tfrac{3}{2}\rangle_z\}$$

$$+ N_{lh}\{|\tfrac{3}{2}, +\tfrac{1}{2}\rangle_z + |\tfrac{3}{2}, -\tfrac{1}{2}\rangle_z\},$$

$$N_{hh} = \frac{-\sqrt{3}\Omega}{\sqrt{2(E_{hh} - E_1)^2 + 6\Omega^2}}, \quad N_{lh} = \frac{E_{hh} - E_1}{\sqrt{2(E_{hh} - E_1)^2 + 6\Omega^2}}. \qquad (10)$$

The corresponding dipole matrix element is

$$|\langle \tfrac{1}{2}, -\tfrac{1}{2}|\sigma + \pi|VB\rangle_x|^2 = 2(N_{hh}^2 + \tfrac{1}{3}N_{lh}^2)M, \qquad (11)$$

where the dipole operators are $\pi = e\hat{x}$ and $\sigma = e\hat{y}$. The relative oscillator strength of the lowest Voigt transition as a function of magnetic field, calculated using Eqs. (9) and (11), is plotted in Fig. 5(b) as the solid line. At low fields (i.e.,

magnetic-field perturbation is negligible compared to strain perturbation) the differences between Faraday and Voigt geometry are small as the Voigt valence-band state is basically also $|\tfrac{3}{2}, -\tfrac{3}{2}\rangle_z$. Therefore the intensities of Mn PL as well as excitonic PL are similar for the two geometries. At higher fields the Voigt oscillator strengths becomes smaller compared to the Faraday value due to the light-hole admixture. The experimentally determined relative PL intensity for the Voigt configuration is even smaller, which is caused by the enhanced energy transfer due to the increased lifetime of the Voigt excitonic state compared to that in Faraday. The details will be discussed in the next section.

B. Discussion of possible energy-transfer mechanisms

The key results concerning the intralayer energy transfer from the excitonic states into the Mn subsystem can be summarized as follows: (i) The intensity of the Mn band and the inverse transfer time $\tau_{transfer}^{-1}$ decrease rapidly with increasing effective field B_{eff} up to a critical value $B_{eff} \approx 0.6$ T/K. This is accompanied by a corresponding increase of the excitonic intensity. (ii) A clear excitonic excitation band is detectable on the Mn band. The position of this excitonic band is shifted to higher energies compared to the corresponding PLE band detected on the excitonic PL. This blueshift vanishes also at a critical value $B_{eff} \approx 0.6$ T/K. (iii) In the QD sample the energy transfer is less efficient than in the corresponding parent sample A, although the dependence on B_{eff} of the relative change of the PL intensities as well as that of the excitonic decay times are basically the same in both samples. (iv) The energy transfer becomes less efficient with increasing temperature. (v) The energy transfer is different in Faraday and Voigt configuration. For intermediate effective magnetic fields, as a result of the magneto-optical anisotropy, the Mn-PL in Voigt-geometry is stronger.

The strong magnetic-field dependence of the intralayer energy-transfer process suggests that spin conservation plays a major role in the overall process. The subprocess within the Mn^{2+} $3d^5$ shell (i.e., the excitation of an electron from the $^6A_1$ ground state to the $^4T_1$ first excited state) is not an allowed dipole transition and requires $\Delta S|_{Mn} = -1$. To make the overall process dipole like (i.e., conserve the total spin $\Delta S_{tot} = 0$) the corresponding subprocess in the excitonic system should yield $\Delta S|_{exc} = +1$. Possible mechanisms which fulfill these requirements are schematically depicted in Fig. 6. The mechanism, which obviously dominates in our samples, is the energy transfer via donor-bound excitons D^0X shown in Fig. 6(a). A bright exciton alone such as $e2 + h$ in Fig. 6(a) can only contribute a subprocess $\Delta S|_{exc} = 0$ when transferring by recombination its energy into the Mn subsystem. Therefore the total spin balance would be $\Delta S_{tot} = -1$ and spin conservation would be violated. The situation changes in the case of a D^0X complex comprising the donor ion D^+, an electron $e1$ bound to it and the donor-bound exciton $e2 + h$. Within the D^0X complex the hole h can recombine with $e1$, instead of $e2$, yielding a spin contribution of the subprocess of $\Delta S|_{exc} = +1$ and thus allowing the conservation of the total spin $\Delta S_{tot} = 0$.
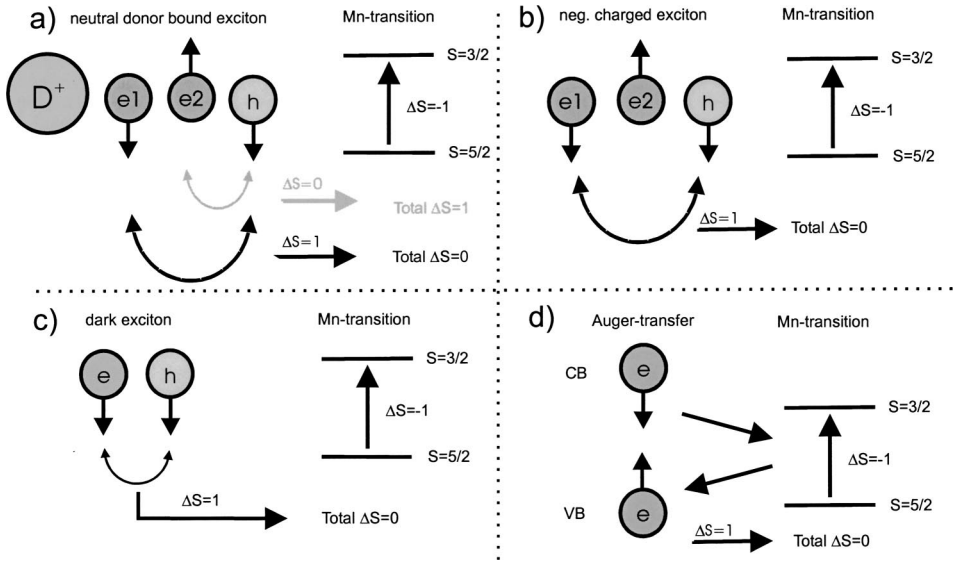
FIG. 6. Schematic diagrams of possible mechanisms for intralayer energy transfer from the excitonic states into the Mn internal transitions, for which the total spin is conserved. (a) Exciton bound to a neutral donor D^0X; (b) negatively charged exciton X^-; (c) dark (triplet) exciton; (d) Auger-transfer process.

Within this D^0X picture all the key observations listed at the top of this section can be explained. On applying an external magnetic field, the D^0X complex becomes destabilized.[27] The formation of a D^0X complex requires the spin of the exciton electron $e2$ ($\uparrow$) and that of the electron bound to the neutral donor $e1$ ($\downarrow$) to be antiparallel as both electrons occupy the same state in real space. With increasing magnetic field the effective binding energy ΔE_B between the FX and the D^0X state decreases. At a critical magnetic field strength B_c, it is energetically favorable for the D^0X complex to decay into a free exciton with electron spin $\downarrow$ and a neutral donor D^0 whose electron also has also spin $\downarrow$. The critical magnetic field can be estimated using

$$\Delta E_B(B_c) = E_D - \tfrac{5}{2} N_0 \alpha x a B_{5/2}(B_c, \Theta) = 0, \qquad (12)$$

where E_D is the binding energy of the exciton bound to the neutral donor in zero-magnetic field and the second term describes the splitting of the two spin components of the conduction-band states in an external magnetic field where $N_0\alpha$ is the s-d exchange integral of the Γ_6 conduction band. Assuming typical E_D values between 5 and 7 meV,[28] and using typical magnetic-field shift measured for the samples under study together with $|N_0\alpha|:\|N_0\beta| \approx 1:6$,[12,17] one obtains critical effective-field values B_{eff} values in the range 0.5 and 0.9 T/K for the samples.[29,30] The observed critical effective fields B_{eff} for the energy transfer from the excitonic states into the Mn $3d^5$ shell given under key results (i) and (ii) are all within this range. At zero field and a constant temperature, the occupation of the D^0X state is highest. With increasing B_{eff} the effective binding energy of the exciton to the D^0 is reduced and more and more of the D^0X thermally dissociate into D^0 and a free exciton until above the critical effective field basically all D^0X are dissociated. This is in full agreement with the intensity behavior of the Mn-PL band and the excitonic PL emission summarized in (i). Similarly, the drop of the ratio of Mn intensity to excitonic intensity (i.e., a less efficient energy transfer) with increasing temperature under (iv) can be also explained as an increasing thermal dissociation of the D^0X into D^0 and free exciton. The blue-

shift between the excitonic PLE signals detected on the excitonic PL and the Mn PL and the magnetic-field dependence of this blueshift under point (ii) can also be related to the D^0X. When the crystal is excited by photons electron-hole pairs are created. These can either relax to the bottom of the excitonic density-of-states ($k = 0$ for the center-of-mass motion) and recombine as a free exciton or are captured by a D^0 and recombine as a D^0X. The bigger the k of the exciton (i.e., its excess energy) the greater the mean lateral distances it can travel in the crystal. Thus the higher the k the more likely the exciton is captured by a D^0 before recombination. The excitonic PLE signal detected on the excitonic PL basically reflects the density of states of the free excitons. In this case, there is effectively no influence of the donor-bound excitons as the corresponding density of states is several orders of magnitude smaller. However, the influence of the D^0X cannot be neglected in the case of the PLE signal detected on the Mn PL as the energy transfer into the Mn $3d^5$ shell from a D^0X is far more efficient than from a free exciton because of the possibility of conserving the total spin in the former case. Therefore the corresponding PLE signal consists of a contribution from the free excitons and an additional contribution due to the D^0X because the products of occupation number and transfer probability for free excitons and D^0X become comparable. The PLE signal of the free excitons is similar to that detected on the excitonic PL. The additional contribution due to the D^0X is shifted to higher energies because of the k dependence of the probability of forming a D^0X complex. At zero-magnetic field this second contribution causes the difference between the PLE signals detected on the excitonic and the Mn PL. As the magnetic field is increased and the D^0X is destabilized, the second contribution decreases and finally vanishes leading to the effects described under (ii). Another important point is result (iii), i.e., the energy transfer in the QD sample is less efficient than in the parent sample A, although the magnetic-field dependence of the energy transfer is similar. This is related to the fact that at the low donor concentrations of sample A the nanofabrication of the QD pillars yields

statistically many pillars where the semimagnetic $Zn_{0.75}Cd_{0.16}Mn_{0.09}Se$ layer does not contain a D^0.[20,30] Therefore these pillars cannot show any $3d$ emission caused by an energy transfer from D^0X to the Mn^{2+} ions. This leads eventually to the weaker $^4T_1$ to $^6A_1$ emission band in the QD sample. Finally, the magnetic-field dependence of the Mn-PL intensity in Voigt geometry is stronger than in Faraday geometry in an intermediate range of effective magnetic fields as summarized under (v). The increasing decay time in Faraday configuration [see Fig. 5(a)] up to the critical field is in agreement with the D^0X related energy transfer. After suppression of this path at higher fields the decay time saturates at $\tau \approx 45$ ps. The corresponding $\tau_{transfer}$ of about 180 ps is related to the remaining direct transfer from the excitonic states into the Mn $3d^5$ shell which does not show any field dependence. From Fig. 3(a) one can see that it is about 25% of the total transfer. The mechanism of this non-field-dependent transfer is not clear but should be connected with a relaxed spin selection rule.

The higher Mn PL in Voigt configuration in the intermediate field range [inset of Fig. 5(a)], which corresponds to the lower decay times τ [Fig. 5(a)] is caused by the reduced transition probability of the lowest excitonic state in Voigt and a respective increased radiative lifetime of the excitonic state in this geometry due to the light-hole admixture. Thus even assuming an unchanged transfer time τ_{Mn} in Voigt geometry compared to the Faraday configuration, the energy transfer into the Mn system is increased. It should be noted that both transfer channels, the D_0X channel at low fields as well as the remaining direct transfer at higher fields, are enhanced by the increased life time in Voigt geometry. This also explains the lower experimentally observed excitonic emission intensity depicted in Fig. 5(b) compared to the calculated transition probability, as the radiationless energy transfer into the $3d$ shell is not included. Other excitonic complexes which allow a spin balance $\Delta S|_{exc} = +1$ of the excitonic subprocess are the negatively charged exciton X^- and the dark exciton given in Figs. 6(b) and (c), respectively.

In the case of quantum well samples (even when nominally undoped, i.e., with donor concentrations between 10^{15} and 10^{16} cm^{-3} as in our samples), the existence of X^- cannot be entirely ruled out.[28] However, X^- are usually only clearly identified at much higher donor concentration in II-VI materials of the order 10^{20} cm^{-3}.[31,32] Nevertheless, it is very hard to distinguish between effects due to donor-bound excitons D^0X and charged excitons X^- in luminescence. This also holds in the case of the intralayer energy transfer from the excitonic states into the Mn $3d^5$ states as existence of X^- is *per se* correlated with the existence of donors in the samples and the destabilization of the X^- by an external magnetic field is described also by Eq. (12). However, it is known that the binding energy E_D of the electron $e1$ to the exciton $e2 - h$ is smaller than that of an exciton to a D^0. Typical E_D values for X^- are 2–4 meV,[28,33] corresponding to a critical effective fields $B_{eff} \approx 0.15 - 0.4$ T/K which are considerably smaller than the B_{eff} values observed in our experiments. Therefore we believe that in our samples this process does not play a dominant role in the energy transfer into the Mn $3d^5$ states.

The energy-transfer process via dark excitons is also very unlikely to play a dominant role in our samples. The dark exciton state is known to be about only 0.5 meV lower in energy than the singlet exciton in samples comparable to the samples under study.[34] The lowest dark exciton shifts with magnetic field proportional to $(-N_0\alpha - N_0\beta)$ whereas the lowest singlet exciton state shifts proportional to $(N_0\alpha - N_0\beta)$ yielding a critical $B_{eff} \approx 0.1$ T/K for the crossover of the energies of dark and bright exciton in the field. Above this critical B_{eff} the occupation number of the dark exciton level decreases rapidly and this energy process would be suppressed. This critical effective field value is much lower than the value of 0.6 T/K observed in our experiments indicating that this is not the main energy-transfer mechanism in our samples. Furthermore the existence of dark excitons should not be affected by the nanofabrication process, i.e., observation (iii) cannot be explained.

Figure 6(d) depicts a mechanism which has been suggested by Nawrocki *et al.*[35] It is an Auger-like process where an electron with a spin opposite to those of the five electrons in the $^6A_1$ ground state is virtually absorbed by the $3d^5$ shell of that Mn ion and an electron of opposite spin is emitted from the $3d^6$ shell into the valence band. This effect will be suppressed on application of an external magnetic field as the conduction-band electron states split in the magnetic field such that the lower electron state has the same spin orientation as the $S = \frac{5}{2}$ spin of the Mn^{2+} ion. We do not believe that this energy-transfer mechanism is dominant in our samples as it cannot explain the reduction of the energy transfer in the QD compared to the parent sample. Also the Auger process would possibly be more effective with increasing temperature in contradiction with our findings.

It should also be noted that the observed magnetic-field behavior of the $^4T_1 - ^6A_1$ emission is not caused by a weakening of the resonance between the $Zn_{0.75}Cd_{0.16}Mn_{0.09}Se$ excitonic emission and the broad Mn^{2+} absorption bands. The internal Mn transitions are known to exhibit only a small magnetic-field dependence. Comparing with the results for the Mn absorption of a polycrystalline film of MnSe in Ref. 36 or in $Zn_{1-x}Mn_xSe$ in Ref. 9, we find that with increasing magnetic field the $Zn_{0.75}Cd_{0.16}Mn_{0.09}Se$ excitonic emission energy shifts along a range of increasing Mn absorption, which should increase the transfer rate. Summarizing the above discussion we are convinced that the dominant energy-transfer mechanism in our samples is that via the D^0X complex.

IV. INTERLAYER ENERGY TRANSFER

A. Experimental findings

Figure 7 depicts PL spectra in the excitonic region of the two ADQW structures B and C excited with energies above the ZnSe barrier. As the intermediate ZnSe barrier is only 6 nm wide, the excitonic states of the NMW and the DMW are coupled in both samples. For sample B the excitonic PL is dominated by the D^0X emission from the NMW and there is no emission from the DMW at all fields due to a fast tunneling or relaxation from DMW excitons into the NMW. The situation is different for sample C. At zero field the excitonic
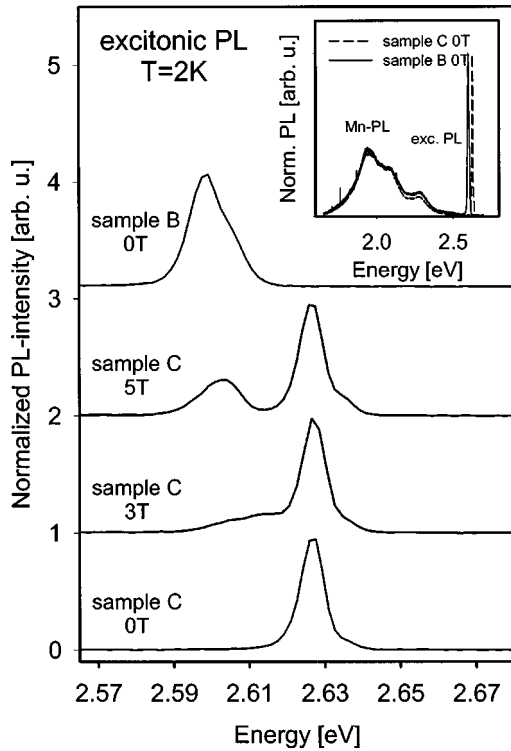
FIG. 7. PL spectra of the excitonic PL of the asymmetric double quantum well (ADQW) structures at zero field for sample B and at various magnetic fields for sample C. $T = 2$ K. Inset: PL spectra at zero field of the two samples showing the spectral range of the excitonic and the Mn PL. $T = 2$ K.

PL is again dominated by the D^0X emission of the NMW. However, in Faraday geometry, with increasing magnetic field a second emission band is observed and shifts strongly to lower energies. It corresponds to the excitonic emission from the DMW. Energy-transfer and tunneling processes between the excitonic states of such samples have been studied in great detail in Refs. 4 and 5. Here, we will focus on the

energy transfer from the coupled excitonic states of the DMW and the NMW into the internal $3d^5$ shells of the Mn ions localized solely in the DMW. That an energy transfer from the excitonic states into the Mn subsystem takes place in both samples is shown in the inset of Fig. 7. For both samples a strong orange Mn PL is clearly visible in addition to the sharp excitonic PL bands.

Figure 8 shows PLE spectra detected on the Mn PL for both samples. The spectra were acquired at various magnetic fields up to 7 T in Faraday as well as in Voigt geometry. We will first discuss sample B. In both field geometries, it can be seen that the PLE signal of the heavy-hole (hh) exciton of the DMW splits and shifts strongly with increasing magnetic field whereas the PLE signal of the hh exciton of the NMW does hardly change. The main difference between the two samples is that in sample C the lowest excitonic state of the DMW crosses that of the NMW whereas in sample B the lowest excitonic state of the DMW is at all fields higher in energy than that of the NMW. We will see in the following that this has consequences for the strength of energy transfer into the Mn system as a function of magnetic field. The energies of the lowest excitonic transitions of the two QW's derived from the PLE experiments in Voigt and Faraday geometry are given in the upper and lower graph of Fig. 9 for samples B and C, respectively. The arrows in the lower graph denote the magnetic field B_X where the crossing of the excitonic states takes place for sample C. This crossing point occurs at a higher field of about 2.1 T in Voigt geometry compared to about 1.6 T in Faraday geometry because of the magneto-optical anisotropy of the excitons of the DMW.

Figure 10 depicts the change of the intensity of the orange Mn PL as a function of magnetic field for Faraday and Voigt geometry when resonantly exciting the excitonic states of the NMW. The top and bottom graph show the results for samples B and C, respectively. For both samples there is a significant Mn-PL signal in zero magnetic field although the energy of the laser excitation is much lower than that of the lowest excitonic state of the DMW, i.e., basically the laser is
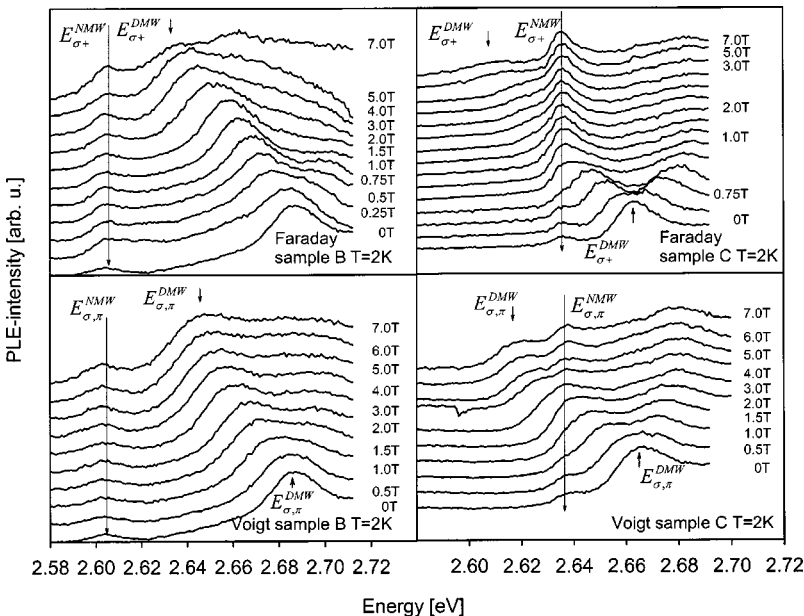

FIG. 8. Faraday and Voigt magneto-PLE spectra of the excitonic region of the ADQW's detected on the Mn PL for sample B and sample C, respectively. $T = 2$ K.
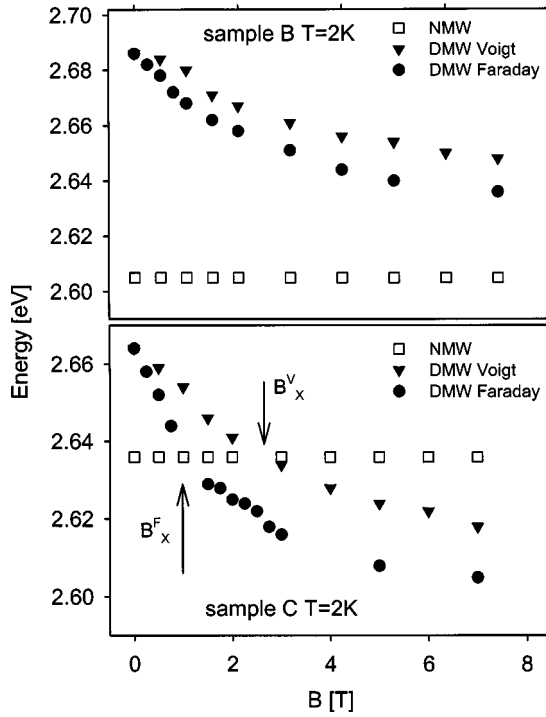
FIG. 9. Magnetic-field dependence of the lowest excitonic transition of the nonmagnetic well (NMW) and the dilute-magnetic well (DMW) in Faraday and Voigt geometry of the two ADQW samples. $T = 2$ K. B_X^F and B_X^V denote the magnetic fields where the transition energies of the lowest transition of the DMW and of the NMW are equal in Faraday or Voigt geometry, respectively.
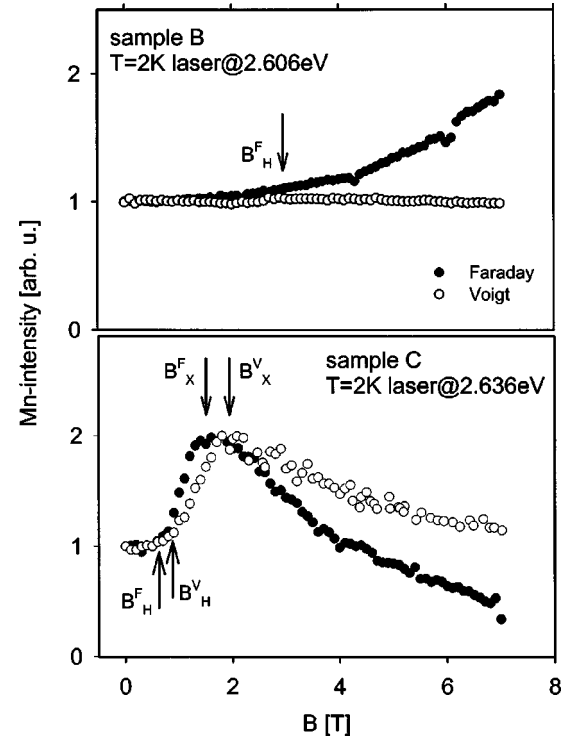

FIG. 10. Magnetic-field-induced change of the intensity of the Mn PL for resonant excitation of the NMW of the ADQW structure in Faraday (●) and Voigt (○) geometry. The results for samples B and C are shown in the upper and lower graph, respectively. B_H^F and B_H^V denote the magnetic fields where the hole states of the NMW and the DMW are equal in Faraday and Voigt geometry, respectively. B_X^F and B_X^V denote the magnetic fields where the transition energies of the lowest transition of the DMW and of the NMW are equal in Faraday or Voigt geometry, respectively.

not absorbed in the (Zn,Cd,Mn)Se layer as the internal self-absorption of the Mn $3d^5$ shell is negligible. Therefore the strong Mn PL must arise from a radiationless resonance energy transfer from the excitonic states of the NMW into the Mn system. It is worth noting that this energy transfer takes place although the excitons and the Mn ions are spatially separated, which seems to be an indication for a dipolar-type energy transfer. For sample B with increasing magnetic field, the Mn-PL intensity is virtually constant in Voigt geometry, whereas in Faraday geometry it starts to increase significantly for magnetic fields above $B_c \approx 3$ T. The intensity of the Mn PL at the highest magnetic field is twice that at zero field. For sample C, the magnetic-field behavior of the intensity of the Mn PL when resonantly exciting the NMW is very different from sample B. Already at low magnetic fields of about 0.8 T there is a rapid increase of the Mn emission. A maximum occurs at 1.6 T for Faraday geometry and at 2.0 T for Voigt-geometry. After the maximum the Mn PL decreases again with increasing magnetic field. This decrease is more pronounced in Faraday geometry than in Voigt geometry. The magnetic fields where the maxima occur agree fairly well with the crossing fields B_X derived from Fig. 9.

B. Discussion

To understand magnetic-field dependence of the intensity of the Mn PL when exciting resonantly the NMW one has to consider the magnetic-field-induced changes of the excitonic

states of the two coupled QW's. In contrast to the intralayer energy transfer from the excitonic states into the Mn system discussed in Sec. III, the interlayer energy transfer discussed here depends strongly on the modification of the valence-band structure of the ADQW by the external magnetic field. Three different scenarios depicted in Fig. 11 may occur. In scenario (1) the lowest excitonic state is that of the NMW. When resonantly exciting this state the electron and hole states of the DMW are not involved in the recombination process. The excited electron-hole pairs of the NMW may contribute to the observed PL by either recombining radiatively or by transferring their energy by a Dexter-Förster-type transfer into the $3d^5$ shells of the spatially separated Mn ions located in the DMW. Scenario (2) might occur already at moderate magnetic fields. Because of the rather small valence-band offset between the two QW materials and the strong p-d induced giant Zeeman shift of the valence-band states it happens that with increasing magnetic field the lowest valence-band state of the ADQW is no longer situated in the NMW but in the DMW. Again, when resonantly exciting the NMW, the DMW cannot be directly excited. However, some of the holes will tunnel from the NMW into the DMW leading to two possible radiative recombination pathways for
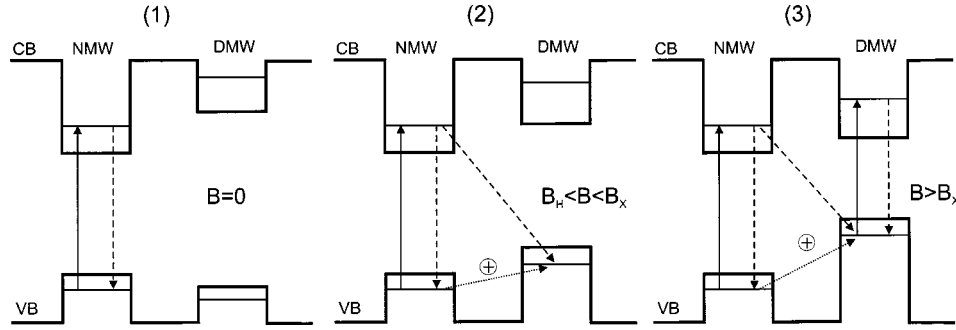
FIG. 11. Three possible scenarios (1)–(3) of the band alignment of an ADQW structure in the magnetic field. The dashed arrows indicate the excitonic transitions which are possible when resonantly exciting the NMW (solid line). The dotted line indicates a relaxation (tunnelling) of holes from the NMW into the DMW. B_H denotes the magnetic field where the hole states of the NMW and the DMW are equal in energy. B_X denotes the magnetic field where the transition energies of the lowest transition of the DMW and of the NMW are equal.

the QW excitons either a direct recombination in the NMW or an indirect recombination involving the electron state of the NMW and the hole state in the DMW. This indirect exciton will have a very long radiative lifetime. In addition, the corresponding hole state as it is localized in the DMW has a large overlap with the Mn ions and the corresponding electron in the NMW might be bound to a D^0 more or less independent of the magnetic field. Therefore it can be anticipated that the energy transfer from these indirect exciton states into the $3d^5$ shells of the Mn ions will be extremely efficient. On increasing the magnetic field further scenario (3) might occur. In this scenario the energy of the lowest excitonic state of the DMW is lower than that of the NMW. Both QW's will be excited directly when exciting resonantly the NMW, but the excitation of the upper DMW might be somewhat higher. Thus, in addition to the excitonic transitions discussed for the two previous scenarios, a direct excitonic recombination in the DMW accompanied by the corresponding intralayer energy transfer might take place. Due to this new recombination path the mean life time of the holes in the DMW will be drastically reduced leading to an effective suppression of the formation of indirect excitons. For sample B in Voigt geometry the band alignment of the ADQW structure always corresponds to scenario (1) explaining the constant intensity of the Mn PL as a function of magnetic field. In Faraday geometry, because of the larger magnetic-field shift of the lowest hole state compared to Voigt geometry, a change from scenario (1) to scenario (2) takes place at a magnetic field $B_H \approx 3$ T leading to the significant increase of the intensity of the Mn PL due to the efficient energy transfer from the indirect excitons whose number keeps increasing with increasing magnetic field due to an increasing relaxation probability into the indirect exciton state compared to the rather unchanged transition probability in the NMW. Scenario (3) is never reached for this sample up to 7 T (see Fig. 9).

With increasing magnetic field all three scenarios occur for sample C in Faraday as well as in Voigt geometry. Up to about 0.5 T the Mn intensity is fairly constant corresponding to scenario (1). Increasing the magnetic field further, scenario (2) occurs first in Faraday geometry and at a slightly higher magnetic field in Voigt geometry leading to the rapid rise of the Mn intensity. This rise is steeper in the Faraday

geometry as the stronger magnetic-field shift of the lowest hole state favors the formation of indirect excitons. For the same reason the crossing point of the lowest excitonic transitions B_x of the two QW's occurs at a lower field in Faraday than in Voigt geometry. This crossing point corresponds to the maximum of the Mn intensity in both geometries. Above B_x the band alignment of the ADQW corresponds to scenario (3), i.e., the energy transfer due to the indirect exciton is overwhelmed by the absorption of the DMW and a magnetic-field dependence of the Mn intensity dominated by intralayer transfer from the excitonic states of the DMW into the Mn system is observed. The difference between Faraday and Voigt geometry in this case occurs because the transition from scenario (2) to (3) occurs at higher field strengths as the absorption of the DMW shifts weaker in Voigt geometry as in Faraday geometry as previously mentioned.

V. CONCLUSIONS

The intralayer energy transfer from excitonic states into the Mn $3d^5$ shell in wide-gap (II,Mn) VI semiconductors is a Dexter-Förster-like radiationless resonance energy-transfer process. It is shown that this transfer is strongly enhanced if the total spin of the overall process is conserved, $\Delta S_{\mathrm{tot}} = 0$. As the subprocesses within the Mn system (i.e., the internal Mn transitions involving $S = \frac{3}{2}$ excited states and the $S = \frac{5}{2}$ ground state) are basically dipole forbidden, $\Delta S|_{\mathrm{Mn}} = -1$, the corresponding process within the excitonic subsystem requires $\Delta S|_{\mathrm{exc}} = +1$ to conserve the total spin. This requirement is not fulfilled by a bright exciton, however, several other excitonic complexes which fulfill this requirement may be anticipated. Possible candidates are dark excitons, donor-bound excitons D^0X or negatively charged excitons X^- (trions) or an Auger-like process. In our samples, the careful analysis of the magnetic-field and time dependence of the excitonic and Mn luminescence gives evidence that the D^0X complex plays a dominant role in the intralayer energy transfer.

In more complex structures, containing coupled nonmagnetic and dilute-magnetic quantum wells, the excitonic band

structure can be continuously tuned by an external magnetic field. In such samples, there is a competition between the intralayer energy-transfer processes and interlayer energy-transfer processes. These interlayer processes take place between the Mn ions situated in the DMW and indirect excitons (where the hole is confined in the DMW and the electron confined in the NMW) as well as direct excitons of the NMW. The continuous magnetic-field tuning demonstrates convincingly the subtle interplay of excitonic band structure of the ADQW and spin effects in the energy-transfer processes.

*Corresponding author: Dr. P. J. Klar. Fax: ++49(0)6421 2827036; e-mail address: klarp@mailer.uni-marburg.de

[1] I. Lawrence, S. Haake, H. Mariette, W. W. Rühle, H. Ulmer-Tuffigo, J. Cibert, and G. Feuillet, Phys. Rev. Lett. **73**, 2131 (1994).

[2] K. Hieke, W. Heimbrodt, I. Lawrence, W. W. Rühle, Th. Pier, H. E. Gumlich, D. E. Ashenford, and B. Lunn, Solid State Commun. **93**, 257 (1995).

[3] V. V. Rossin, J. Puls, and F. Henneberger, Phys. Rev. B **51**, 11 209 (1995).

[4] W. Heimbrodt, L. Gridneva, M. Happ, N. Hoffmann, M. Rabe, and F. Henneberger, Phys. Rev. B **58**, 1162 (1998).

[5] W. Heimbrodt, M. Happ, and F. Henneberger, Phys. Rev. B **60**, R16 326 (1999).

[6] U. Stutenbäumer, H. E. Gumlich, and H. Zuber, Phys. Status Solidi B **156**, 561 (1989).

[7] D. Leinen, Phys. Rev. B **55**, 6975 (1997).

[8] D. Some and A. V. Nurmikko, Phys. Rev. B **48**, 4418 (1993).

[9] H. Waldmann, C. Bennecke, W. Busse, H. E. Gumlich, and A. Krost, Semicond. Sci. Technol. **4**, 71 (1989).

[10] R. E. Kellog, J. Lumin. **1/2**, 435 (1997).

[11] O. Goede, W. Heimbrodt, and V. Weinhold, Phys. Status Solidi B **136**, K49 (1986).

[12] O. Goede and W. Heimbrodt, Phys. Status Solidi B **146**, 11 (1988).

[13] W. Heimbrodt, C. Benecke, O. Goede, and H.-E. Gumlich, Phys. Status Solidi B **154**, 405 (1989).

[14] W. Busse, H.-E. Gumlich, B. Meissner, and D. Theis, J. Lumin. **12/13**, 693 (1976).

[15] U. Pohl and H.-E. Gumlich, Phys. Rev. B **40**, 1194 (1989).

[16] O. Goede, W. Heimbrodt, and D. D. Thong, Phys. Status Solidi B **126**, K159 (1984).

[17] J. K. Furdyna, J. Appl. Phys. **64**, R29 (1988).

[18] B. König, I. A. Merkulov, D. R. Yakovlev, W. Ossau, S. M. Ryabchenko, M. Kutrowski, T. Wojtowicz, G. Karczewski, and J. Kossut, Phys. Rev. B **61**, 16 870 (2000).

[19] P. J. Klar, D. Wolverson, B. Lunn, D. E. Ashenford, and T. Henning, Semicond. Sci. Technol. **11**, 1863 (1996).

[20] P. J. Klar, D. Wolverson, J. J. Davies, W. Heimbrodt, M. Happ, and T. Henning, Phys. Rev. B **57**, 7114 (1998).

[21] C. S. Kim, M. Kim, S. Lee, J. Kossut, J. K. Furdyna, and M. Dobrowolska, J. Cryst. Growth **214/215**, 395 (2000).

[22] B. Kuhn-Heinrich, W. Ossau, E. Bangert, A. Waag, and G. Landwehr, Solid State Commun. **91**, 11 (1994).

[23] D. Suisky, W. Heimbrodt, C. Santos, F. Neugebauer, M. Happ, B. Lunn, J. E. Nicholls, and D. E. Ashendford, Phys. Rev. B **58**, 3969 (1998).

[24] W. Y. Yu, A. Twardowski, L. P. Fu, A. Petrou, and B. T. Jonker, Phys. Rev. B **51**, 9722 (1995).

[25] P. Peyla, A. Wasiela, Y. Merle d'Aubigné, D. E. Ashenford, and B. Lunn, Phys. Rev. B **47**, 3783 (1993).

[26] P. J. Klar, H. Falk, and W. Heimbrodt, Solid State Commun. **116**, 125 (2000).

[27] D. Heiman, P. Becla, R. Kershaw, K. Dwight, A. Wold, and R. R. Galazka, Phys. Rev. B **34**, 3961 (1986).

[28] N. Paganotto, J. Siviniant, D. Coquillat, D. Scalbert, J. P. Lascaray, and A. V. Kavokin, Phys. Rev. B **58**, 4082 (1998).

[29] H. Falk, W. Heimbrodt, P. J. Klar, J. Hübner, M. Oestreich, and W. W. Rühle, Phys. Status Solidi B **229**, 781 (2002).

[30] W. Heimbrodt, H. Falk, and P. J. Klar, J. Lumin. **87−89**, 344 (2000).

[31] G. V. Astakhov, D. R. Yakovlev, V. P. Kochereshko, W. Ossau, W. Faschinger, J. Puls, F. Henneberger, S. A. Crooker, Q. McCulloch, D. Wolverson, N. Gippius, and A. Waag, Phys. Rev. B **65**, 165335 (2002).

[32] V. Ciulin, P. Kossacki, S. Haacke, J. D. Ganière, B. Deveaud, A. Esser, M. Kutrowski, and T. Wojtowicz, Phys. Rev. B **62**, R16 310 (2000).

[33] K. Kheng, R. T. Cox, Y. Merle d'Aubigné, F. Bassani, K. Saminadayar, and S. Tatarenko, Phys. Rev. Lett. **71**, 1752 (1993).

[34] J. Puls and F. Henneberger, Phys. Status Solidi A **164**, 499 (1997).

[35] M. Nawrocki, Yu. G. Rubo, J. P. Lascaray, and D. Coquillat, Phys. Rev. B **52**, R2241 (1995).

[36] W. Heimbrodt, O. Goede, I. Tschetscher, V. Weinhold, A. Klimakov, U. Pohl, K. Jacobs, and N. Hoffmann, Physica B **185**, 357 (1993).